Quantification of integrin receptor agonism by fluorescence lifetime imaging

Maddy Parsons[1,*,‡], Anthea J. Messent[2,*,§], Jonathan D. Humphries[2], Nicholas O. Deakin[2] and Martin J. Humphries[2,‡]

[1]Randall Division of Cell and Molecular Biophysics, King's College London, New Hunt's House, Guys Campus, London, SE1 1UL, UK
[2]Wellcome Trust Centre for Cell-Matrix Research, Faculty of Life Sciences, University of Manchester, Michael Smith Building, Oxford Road, Manchester, M13 9PT, UK

*These authors contributed equally to this work
‡Authors for correspondence (e-mails: maddy.parsons@kcl.ac.uk; martin.humphries@manchester.ac.uk)
§Present address: Department of Oncology, University of Cambridge, Cambridge Research Institute, Li Ka Shing Centre, Robinson Way, Cambridge, CB2 0RE, UK

Accepted 4 October 2007
J. Cell Sci. 121, 265-271 Published by The Company of Biologists 2008
doi:10.1242/jcs.018440

Summary

Both spatiotemporal analyses of adhesion signalling and the development of pharmacological inhibitors of integrin receptors currently suffer from the lack of an assay to measure integrin-effector binding and the response of these interactions to antagonists. Indeed, anti-integrin compounds have failed in the clinic because of secondary side effects resulting from agonistic activity. Here, we have expressed integrin-GFP and effector-mRFP pairs in living cells and quantified their association using fluorescence lifetime imaging microscopy (FLIM) to measure fluorescence resonance energy transfer (FRET). Association of talin with β1 integrin and paxillin with α4 integrin was dependent on both the ligand and receptor activation state, and was sensitive to inhibition with small molecule RGD and LDV mimetics, respectively. An adaptation of the assay revealed the agonistic activity of these small molecules, thus demonstrating that these compounds may induce secondary effects in vivo via integrin activation. This study provides insight into the dependence of the activity of small molecule anti-integrin compounds upon receptor conformation, and provides a novel quantitative assay for the validation of potential integrin antagonists.

Supplementary material available online at
http://jcs.biologists.org/cgi/content/full/121/3/265/DC1

Key words: FRET/FLIM, Integrin, Integrin activation, Antagonist, Microscopy

Introduction

Integrins are cell-adhesion receptors that provide physical support for tissues and enable directed migration during development and tissue homeostasis (van der Neut et al., 1996; Wagner et al., 1996). At the cellular level, integrins spatially compartmentalise signalling events by tethering the contractile cytoskeleton to the plasma membrane and indirectly modulating multiple signalling networks. In mammals, genes encoding 18 α and 8 β integrins produce polypeptides that combine to form 24 heterodimeric receptors (Hynes, 2002), 12 of which contain the β1 subunit. Both subunits are noncovalently associated, type I transmembrane proteins with large extracellular and mostly short cytoplasmic domains. In recent years, substantial progress has been made towards defining the conformational changes that underpin integrin affinity regulation and identifying the effector proteins that initiate integrin signalling (Luo et al., 2007; Humphries, 2000). Transmembrane or cytoplasmic domain separation, triggered either by the binding of FERM domain-containing cytoplasmic proteins (such as talin and myosin X) (Zhang et al., 2004; Tadokoro et al., 2003; Garcia-Alvarez et al., 2003) or extracellular ligands, is currently thought to be the mechanism for the bidirectional transmembrane signal transduction that regulates adhesion (Kim et al., 2003).

In patients with inflammatory and neoplastic diseases, aberrant integrin function perturbs cellular trafficking and causes dysregulation of cellular differentiation (Mousa, 2002). Within the past decade, the first generation of anti-integrin drugs has been approved for human therapy (Leclerc, 2002). Some of these agents are small molecule mimetics of the acidic peptide active sites found in most integrin ligands (e.g. RGD and LDV). Although these agents are potent, competitive inhibitors of integrin-ligand binding in vitro and in vivo, it is now evident that they frequently retain the agonistic properties of their parent ligands. This activity can lead to biological side effects, such as platelet dysfunction, and can consequently impair the drug development process (Hantgan et al., 2007). As a result, there is a pressing need for a reporter assay to measure the agonistic activity of integrin-binding ligands and small molecules in situ. Here, we present such a system, which uses fluorescence resonance energy transfer (FRET) to measure direct integrin-effector binding in intact cells. This assay also has the potential to detect and quantify integrin signalling during normal biological processes, such as migration and differentiation.

Results and Discussion

Initially, a full-length human β1 integrin construct was C-terminally tagged with green fluorescent protein (GFP). Although other β-integrin-GFPs have been described (Ballestrem et al., 2001), β1-integrin-GFP has not been previously generated because the ubiquitous distribution and high endogenous expression of β1 integrin in most cells makes it difficult to express. This construct was therefore stably expressed to endogenous levels in immortalised β1-integrin-null mouse embryonic fibroblasts

(MEFs) and its functional activity tested by a combination of confocal microscopy (to confirm its presence in adhesion complexes) and cell attachment and spreading assays (supplementary material Fig. S1). To identify effectors that might undergo FRET with β1 integrin, four different candidate adhesion complex components were tested, each of which has been reported to bind directly to β integrins: the talin head domain (residues 1-433) (Garcia-Alvarez et al. 2003), talin rod domain (residues 1984-2344) (Xing et al., 2001), α-actinin (Otey et al., 1990) and paxillin (Schaller et al., 1995). β1-integrin-GFP MEFs were transfected with mRFP conjugates of each protein, plated onto a fibronectin substrate and integrin-effector binding analysed using FLIM to measure FRET. This technique enables visualisation and quantification of protein-protein interactions by analysis of the donor lifetime decay kinetics (see Materials and Methods for full description of technique and analysis) (Parsons et al., 2005).

Specific interactions between β1 integrin and the talin rod domain and α-actinin were detected, but no interaction was observed for the talin head domain or paxillin (Fig. 1A). The substrate dependence of the interaction between the talin rod domain and β1 integrin was examined. As shown in Fig. 1B, a modest interaction was detected on both collagen and laminin substrates, but binding was most prominent on fibronectin, where FRET was localised to focal adhesion structures (Fig. 1A). No FRET was detected between the integrin and any of the acceptors in cells plated on a non-integrin-binding poly-L-lysine substrate (PLL; Fig. 1B and data not shown). Although not the primary focus of this study, these data add significantly to our understanding of integrin effectors. Despite some controversy in the literature, it is apparent that the talin rod and α-actinin are able to interact directly with β1 integrin. From other studies, the ability of the talin head to associate with β1 integrin is unequivocal (Garcia-Alvarez et al., 2003), but we failed to detect the association by FRET-FLIM. We speculate that the functional role of the head domain may be transient, and/or restricted to early adhesion complexes only.

Having established that β1-integrin-GFP associates with talin-rod-mRFP, the activation state dependence of the interaction was examined. To constrain

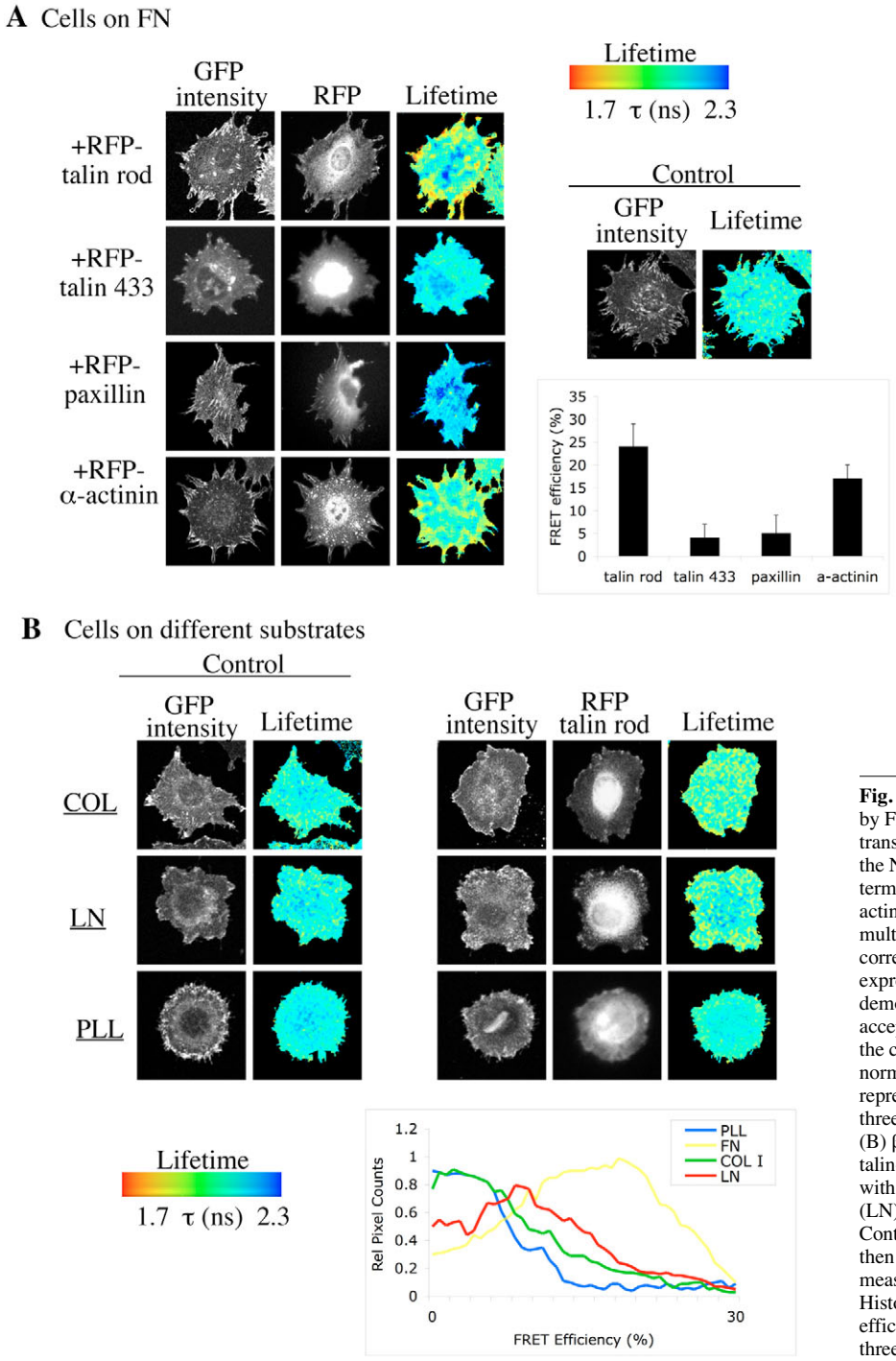

Fig. 1. Interaction of β1 integrin-GFP and talin-rod-RFP by FRET. (A) β1 integrin-GFP fibroblasts were transfected with plasmids encoding mRFP conjugates of the N-terminal 433 amino acids of talin (talin 433), the C-terminal rod domain of talin (talin rod), paxillin or α-actinin and plated onto fibronectin. Images show the GFP multiphoton intensity image and (where appropriate) corresponding widefield CCD camera image of the RFP expression. Control (GFP integrin alone) image demonstrates a normal GFP lifetime in the absence of acceptor. Lifetime images mapping spatial FRET across the cells are depicted using a pseudocolour scale (blue, normal GFP lifetime; red, FRET). The bar graph represents average FRET efficiency of seven cells over three independent experiments. Error bars indicate s.e.m. (B) β1 integrin-GFP fibroblasts were transfected with talin-rod-mRFP. Cells were plated onto coverslips coated with poly-L-lysine (PLL), collagen I (COL), or laminin-1 (LN) and allowed to attach and spread for 2 hours. Control (untransfected) cells or co-transfected cells were then imaged by FLIM to detect FRET. Lifetime measurements were acquired and depicted as in A. Histogram analysis of the spread of relative FRET efficiency is an average of more than eight cells from three different experiments.

the location of the clustered integrin for analysis, β1-integrin-GFP MEFs expressing talin-rod-mRFP were plated onto PLL and incubated with 4.2 μm beads coated with fibronectin ligand or the monoclonal antibodies 12G10 (which detects the high affinity or primed state and stimulates ligand binding) (Mould et al., 1995; Mould et al., 2002), mAb13 (which detects non-ligand-occupied integrin and which blocks ligand binding) (Akiyama et al., 1989) or K20 (which is non-function-altering and detects all conformational states) (Amiot et al., 1986; Mould et al., 2005). As shown in Fig. 2A, an interaction between integrin and talin rod was only observed with fibronectin- or 12G10-coated beads. Confocal analysis of these cells also revealed actin recruitment to the bead structures in those cases where FRET was detected (Fig. 2B). These data suggest that controlling integrin conformation and therefore the activation of the extracellular domain of the integrin, either by native ligand or antibodies alone, can drive recruitment of both talin and actin to the integrin cytoplasmic domain.

To confirm the use of FRET-FLIM for detecting integrin-effector binding, and to generate an assay that might be used to test small molecule inhibitors of integrin function, the previously characterised association between α4 integrin and paxillin (Liu et al., 1999; Goldfinger et al., 2003) was selected. FLIM was used to analyse FRET between α4-integrin-GFP and paxillin-mRFP in both mouse B16F1 and human A375SM melanoma cells. A localised interaction between integrin and paxillin was detected in B16F1 cells plated on fibronectin or an α4-integrin-binding fragment of fibronectin (H/120), but not on PLL (Fig. 3A,B), confirming the results of the previous biochemical analyses. This interaction was also detected in cells plated on VCAM-1 (data not shown). FRET was significantly decreased when two small molecule, LDV ligand mimetic inhibitors of α4β1 integrin [S976162 and S9916197 (Gläsner et al., 2005; Lin et al., 1999) see supplementary material Table S1 and Fig. S2 for characterisation] were added to pre-spread cells (Fig. 3B). Interestingly, the remaining interacting population demonstrated a spatial shift from the cell periphery to the central basal region (just below the nucleus). A similar reduction in α4 integrin and paxillin binding following treatment with these compounds was also seen in live human A375SM melanoma cells plated onto an activated endothelial cell layer (Fig. 3C). These data demonstrate that binding of α4-integrin to paxillin, detected by FRET, is both ligand dependent and sensitive to inhibition with small molecule antagonists.

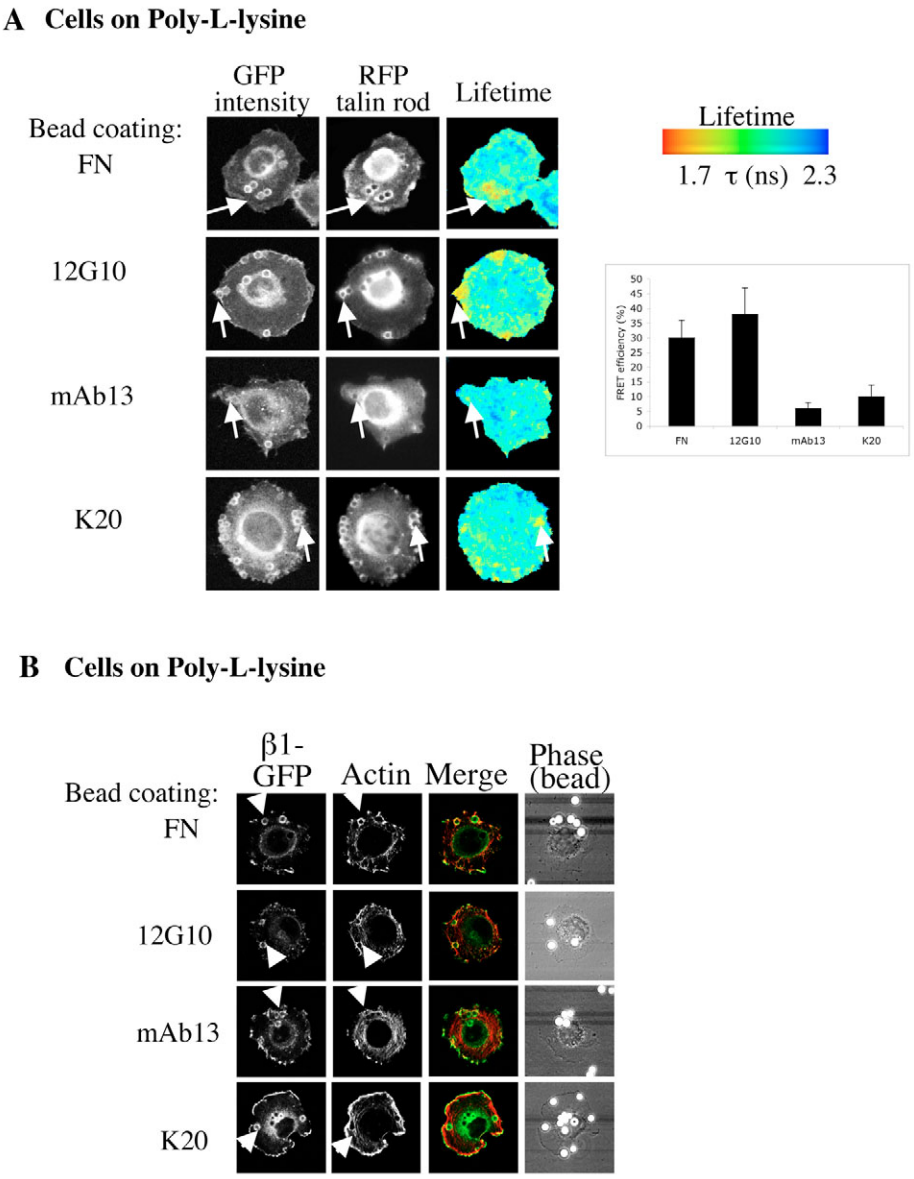

Fig. 2. Ligand regulation of binding of β1 integrin and talin rod. (A) β1 integrin-GFP fibroblasts were transfected with talin-rod-mRFP. Cells were plated onto coverslips coated with poly-L-lysine (PLL), and allowed to attach and spread for 2 hours. Cells were then incubated with 4.2 μm beads coated with FN or anti-β1 antibodies (12G10, mAb13 or K20) for 30 minutes and subsequently imaged using FLIM as in Fig. 1. Bar graph represents average FRET efficiency of 16 cells per ligand. Efficiency was calculated using a mask of constant area around each bead region for local analysis of FRET. Error bars indicate s.e.m. (B) Cells were prepared as in A, and following incubation with beads, samples were fixed, permeabilised and stained with phalloidin-Alexa Fluor 568 to detect F-actin. Cells were then imaged by confocal microscopy.

To test whether the small molecule α4β1 integrin inhibitors could also act as agonists, A375SM cells transfected with α4-integrin-GFP and paxillin-RFP were plated onto PLL and incubated with K20-coated beads. As shown in Fig. 2, these beads cluster, but do not activate integrins. Cells were then treated with vehicle control (DMF) or small molecule α4β1 integrin inhibitors and the interaction between α4 integrin and paxillin assessed by FLIM. Cells treated with either compound demonstrated a significant increase in α4-integrin-paxillin binding at the K20 bead interface (Fig. 4A). This effect was not seen with mAb13 beads, which would be expected to retain the β1 integrin in an

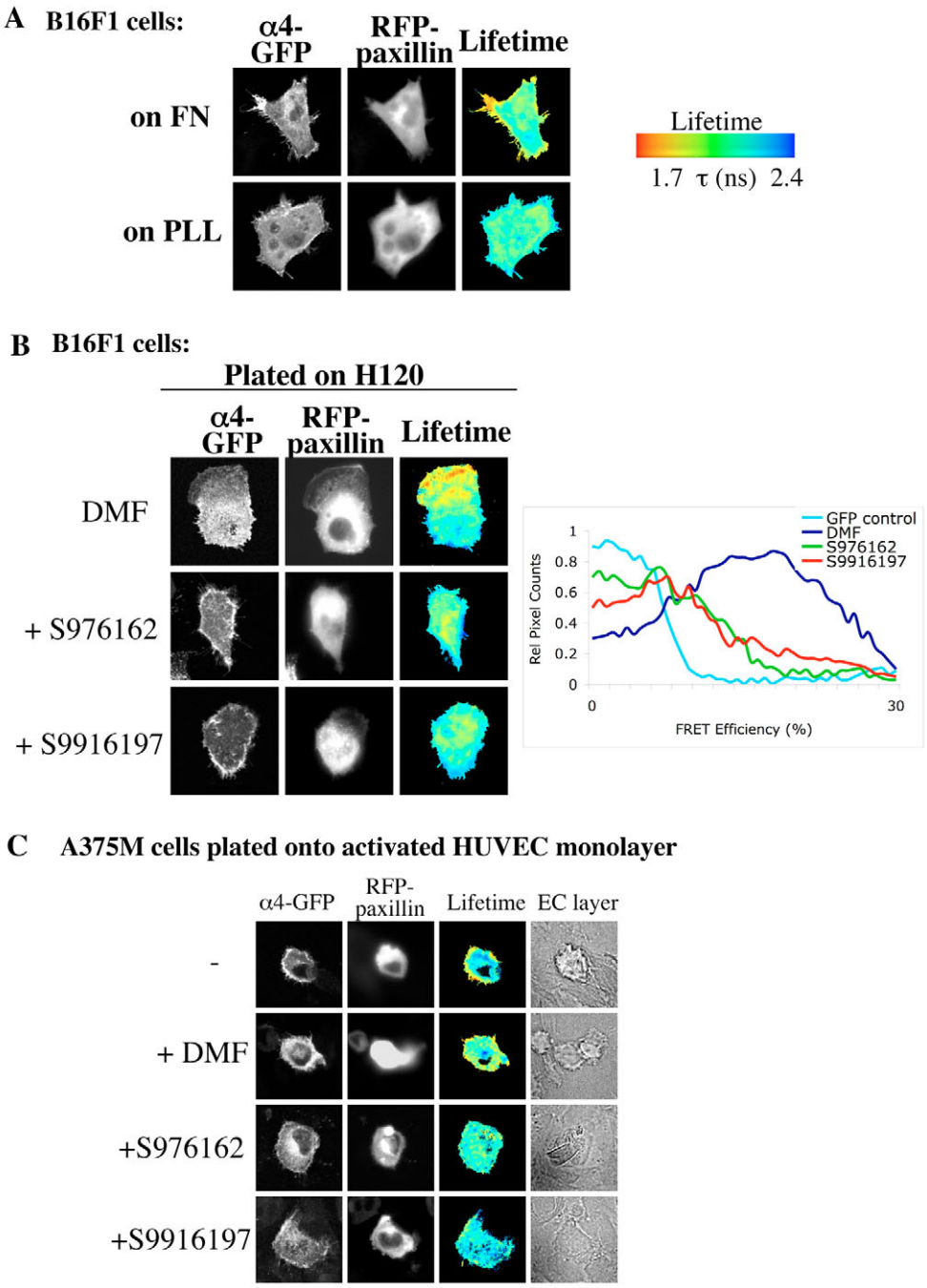

Fig. 3. Ligand binding to the α4 integrin extracellular domain regulates its association with paxillin. (A) B16F1 mouse melanoma cells were transfected with α4-integrin-GFP and paxillin-mRFP. Cells were then plated onto FN- or PLL-coated coverslips and imaged by multiphoton FLIM as before. (B) The same cells were plated onto H120-coated coverslips followed by treatment with DMF vehicle control or stated small molecule inhibitors for 30 minutes and imaged by multiphoton FLIM. Histogram analysis of relative spread of FRET efficiencies is a mean of 18 cells per treatment compared with α4-integrin-GFP alone control. (C) Human A375-SM melanoma cells were transfected with α4-integrin-GFP and paxillin-mRFP and plated onto a monolayer of TNFα-treated activated HUVEC cells. Cells were allowed to adhere for 60 minutes, and were then treated with DMF vehicle control or stated small molecule inhibitors for 30 minutes. Cells were then imaged using multiphoton FLIM as before.

inactive conformation and prevent ligand binding. Moreover, the effects of the compounds were dose dependent in a rank order range that paralleled their anti-adhesive activity (Fig. 4B, supplementary material Table S1, Fig. S2). We interpret these data to indicate that K20 immobilisation of β1 integrin allows the soluble compounds to act as agonists for α4β1 integrin and trigger an activation response in the form of recruitment of cytoskeletal proteins. To extend these findings, an RGD ligand mimetic small molecule inhibitor of α5β1 and αVβ3 integrins (V0519) (Peyman et al., 2000) was tested for its effect on binding of β1-integrin-GFP and talin-rod-mRFP. β1-integrin-GFP cells expressing talin-rod-mRFP were plated onto PLL-coated coverslips and incubated with K20-coated beads in the presence or absence of V0519. As shown in Fig. 4D, V0519 substantially increased the interaction of β1 integrin and talin at the bead interface.

In summary, we have established assays to detect integrin-effector binding by FRET-FLIM. The availability of these assays will not only enable spatiotemporal studies of integrin signalling, but they could also form the basis for low- and high-throughput screening of small molecule inhibitors in the pharmaceutical industry. The application of direct imaging techniques to study small molecule compound effectors in situ may provide an excellent platform for future identification of therapeutic compounds that either possess or lack agonistic activity.

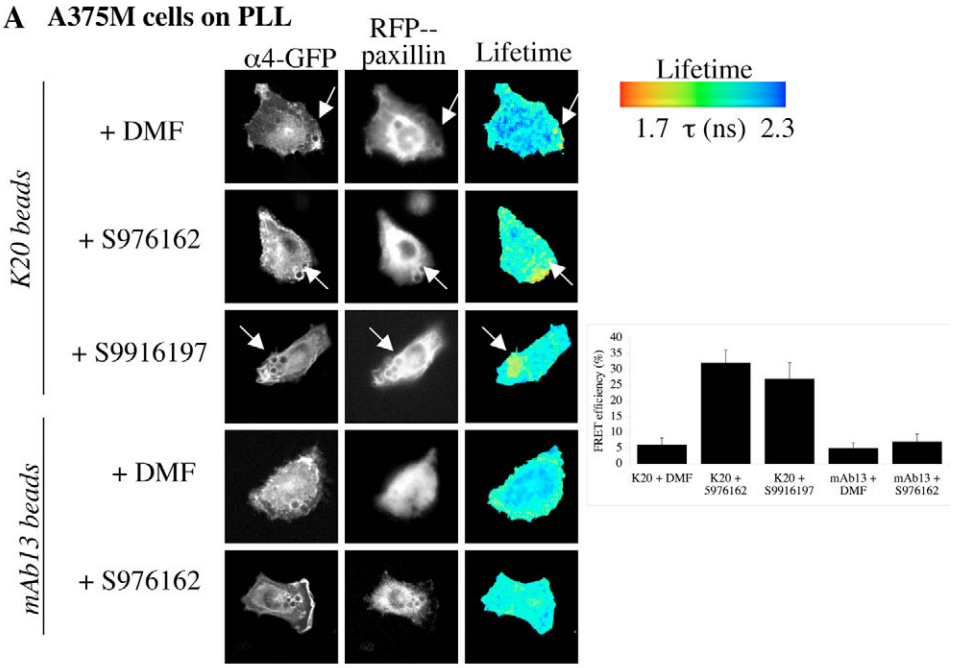

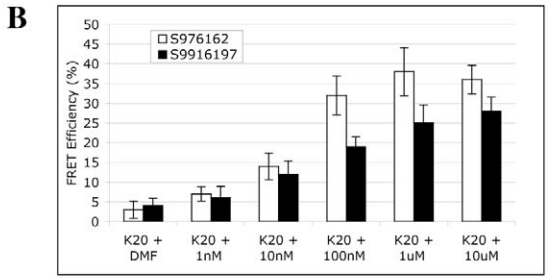

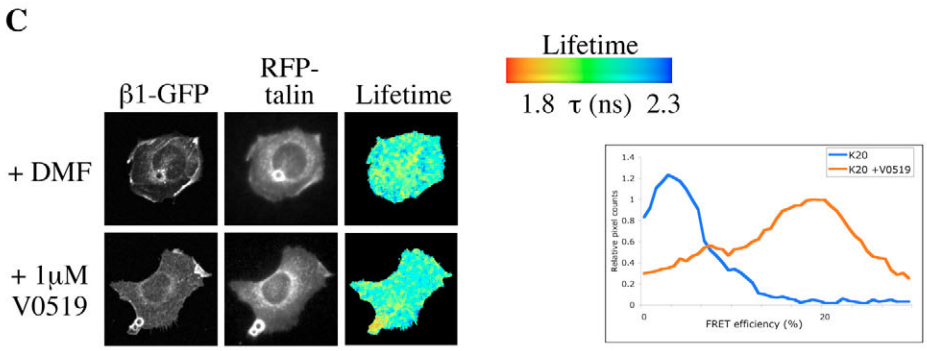

Fig. 4. Small molecule inhibitors induce integrin signalling. (A) A375-SM cells were transfected with α4-integrin-GFP and paxillin-mRFP and plated onto coverslips coated with PLL. Cells were then incubated with K20 or mAb13 antibody-coated beads for 30 minutes, followed by treatment with DMF or small molecule inhibitor as indicated. Cells were then imaged using multiphoton FLIM. Cumulative FRET efficiency data from a masked pre-set region around the bead in ten cells per treatment is shown in the histogram. (B) Histogram demonstrating FRET efficiency of α4-paxillin association at K20 beads over a dose-response range of compounds S976162 or S9916197. Results are means ± s.e.m. (C) β1-integrin-GFP fibroblasts were transfected with talin-rod-mRFP. Cells were then plated onto coverslips coated with PLL and allowed to attach and spread for 1 hour. Cells were then incubated with beads coated with K20 for 30 minutes, and treated with either the vehicle control DMF or V0519 compound, and subsequently imaged using FLIM as before. Cumulative FRET efficiency data from a masked pre-set region around the bead in 12 cells per treatment is shown in the histogram.

Materials and Methods

Plasmid constructs

Generation of talin-mRFP constructs

Full-length mouse talin-1 cDNA was a gift from David Critchley (University of Leicester, Leicester, UK). A 1080 bp fragment corresponding to amino acids 1984-2344 was amplified by PCR using the GGGGGGGAATTCGCTGTGTCTG-GTATCATTGC (forward, F) and AAAAAAGCGGCCGCATTGTTCCTCAA-AGTTC (reverse, R) primers to generate a 5′ *Eco*RI and a 3′ *Not*I restriction site. This region in the talin rod domain has been reported to contain an integrin-binding site (Fragment G) (Tremuth et al., 2004). The PCR product was then cloned into the pcDNA-RFP-C vector (a gift from Roger Tsien, UCSD, CA) to generate a C-terminal monomeric red fluorescent protein tag. Similarly, a 1299 bp fragment corresponding to amino acids 1-433 of talin was amplified by PCR and fused to a C-terminal monomeric RFP tag. This region in the head of the talin protein also contains an integrin-binding site (Calderwood et al., 1999). The primers used were GCAGAATTCCATGGTTGCGCTTTCGCTGAAGGCGCAG (F) and ACATTT-GCGGCCGCTTCCTTTACCGTCCTGAAGGACTGTTGA (R).

Generation of β1-GFP

Full-length human β1A integrin cDNA was the gift of Ken Yamada (NIDCR, NIH, Bethesda, MD). To mutate the stop codon before fusion with a 3′ fluorescent tag, and generate a novel 3′ *Apa*I restriction site, a fragment corresponding to residues 578-799 of the mature sequence was generated by PCR using the primers TTGCAAGTGTCGTGTGTGTG (F) and GTGGATCCCGGGCCCCCCCCCC-TCCTTTTCCC (R). The PCR product was then digested with *Spe*I and *Apa*I. The remaining 5′ portion of β1 was excised from β1-pECE using *Kpn*I and *Spe*I, and both fragments simultaneously ligated into pcDNA3 digested with *Kpn*I and *Apa*I. The fidelity of the resulting construct was confirmed by sequencing (GenBank code XM_005799.1). The mutated, full-length β1 integrin construct was then cloned into pEGFP N1 (Clontech) using *Kpn*I and *Apa*I. The initial 12 amino acid linker between the end of the mature β1 integrin sequence and the start codon of the GFP tag proved

insufficient for mammalian cell expression. Therefore an 18 amino acid linker was constructed. A top strand and a bottom strand oligonucleotide were designed and annealed together, digested with *Apa*I and *Age*I and used to replace the 3′ end of the β1-integrin-pEGFP N1 construct. The resulting linker sequence between the 3′ end of the mature β1 integrin coding sequence and the start codon of GFP was GGGGARRRGQAGDPPVAT. To enable greater flexibility with the colour of the fluorescent tags, the new construct was initially cloned into pHcRed N1 (Clontech) and when a GFP tag was required, the RFP fluorophore was excised using *Age*I and *Not*I, and the GFP sequence from pEGFP N1 cloned into the pHcRed backbone using the same restriction sites. The fidelity of the β1 integrin constructs was verified by sequencing. These constructs were successfully expressed transiently in MEF 7929 ($\beta1^{-/-}$) cells. To maximise the level of stable incorporation of the β1-integrin-GFP DNA in $\beta1^{-/-}$ cells, an additional retroviral construct was used. The β1-integrin-pHcGreen coding sequence was excised from the pHc backbone using *Eco*RI and *Not*I. This coding sequence was ligated into the pFBneo vector (Stratagene) using the same restriction sites, resulting in a construct that produced β1-integrin-GFP-expressing retroviral particles when expressed by amphotropic AM12 packaging cells (a gift from Ian Hart, Cancer Research UK, London, UK).

Generation of α4-GFP

A full-length clone of human α4 integrin in pBluescript (from Yoshi Takada, Dana-Farber Cancer Center, Boston, MA) was used as a backbone. For the generation of α4-GFP, the coding region of the α4-pBluescript was removed and an *Age*I (*Pin*AI) site inserted at the 3′ end using PCR. The α4 cDNA already had a 5′ *Sal*I site and these sites were used to subclone α4 into pECFP-N1. The CFP cassette was then replaced with GFP-N1 to give α4-pEGFP-N1. This was then digested with *Nhe*I and *Not*I positioned 5′ and 3′ to the entire α4-pEGFP and the hyg^+ cassette from pcDNA3.1 hyg^+ ligated using the same restriction sites. PCR primers used to insert a 3′ *Age*I (*Pin*AI) site into the vector backbone were CAA CAG TAA AAG CAA TGA TGA TGG CGG CGG CGG CGG ACC GGT GGA CTT CTT TCA AAT TGA GAG AAT GG and GGA TAG ATA TTA GCT TTC TCC.

Generation of mRFP-paxillin

Full-length paxillin in pEGFPC2 was a gift from Vic Small (IMBA, Vienna, Austria). PCR mutagenesis was carried out using the primers below to insert an *Eco*RI site restriction site at the 3′ end and a 5′ *Hin*dIII site. The primers used were GGA TCC AAG CTT GCC ATG GAC GAC CTC GAC GCC CTG C (F) and GGA TCC GAA TTC CTA GCA GAA GAG CTT GAG GAA GC (R). The PCR product was then sequentially digested and ligated into pcDNA3.1-mRFP-N (from Roger Tsien, UCSD, CA).

Generation of $\beta1^{-/-}$ MEFs

Immortalised β1 $integrin^{-/-}$ murine embryonic fibroblasts were obtained by crossing Immorto mice (Charles River Laboratories, Wilmington, DE) carrying the thermolabile large T antigen H-2KtsA58 (Jat et al., 1991) with mice in which exon 1 of the β1 integrin gene was flanked by loxP sites (Graus-Porta et al., 2001) (a gift of Uli Muller, Friedrich Miescher Institute, Basel, Switzerland) and genotyped by tail-tip PCR. Mice that were homozygous for the wild-type or floxed β1 integrin allele and carried at least one Immorto allele were interbred and E13.5 embryos dissected for MEF preparation. Isolated MEFs were cultured at 33°C in the presence of IFNγ (Sigma; 20 U/ml) for five passages until all non-immortalised cells had senesced. Adenovirus-Cre (AdCreM1; Microbix Inc.) was added at an MOI of 40 overnight to subconfluent cultures of a random subset of cells derived from β1 (fl/fl)/Immorto embryos. Deletion of β1 integrin expression was monitored by flow cytometry with mAb KMI6 (BD Pharmingen) and confirmed by PCR and western blot. Clones from the $\beta1^{-/-}$ MEFs were derived by limited dilution and deletion of β1 integrin was reconfirmed for each clone by flow cytometry.

Retroviral transduction

AM12 packaging cells were maintained in Dulbecco's Modified Eagle's Medium (DMEM) containing 10% FCS. Before transfection, cells were seeded overnight into six-well plates and transfected with 1 μg/well β1-GFP-pFBneo using FuGene 6 reagent (Roche) according to the manufacturer's instructions. 24 hours after transfection, the medium was changed and the transfected cells allowed to condition the fresh medium for a further 48 hours. The conditioned medium was removed, filtered through a 2 μm pore filter, mixed 50:50 with MEF growth medium and placed onto 50% confluent $\beta1^{-/-}$ MEFs. 24-48 hours after adding the retrovirus-containing medium, transduced cells were selected with 0.5 mg/ml neomycin for 10 days then assayed for GFP expression by flow cytometry using untransduced cells as the negative control. In addition to the parent population expressing a mixed level of β1-GFP, a subpopulation of high expressers was isolated by flow cytometry and nine individual clones were derived by limited dilution from these cells.

Cell culture and transient transfection

MEFs were routinely cultured in DMEM, 10% FCS (Sigma) supplemented with 20 U/ml mouse IFNγ (Sigma) at 33°C. For all experiments, MEFs were cultured in growth medium without IFNγ at 37°C to switch off the immortalising gene. B16F1 mouse melanoma cells and A375-SM human melanoma cells were both cultured in DMEM (Sigma) supplemented with 10% FCS, glutamine and penicillin-streptomycin at 37°C. For FLIM experiments, β1-GFP-MEFs, B16F1 or A375-SM melanoma cells were seeded overnight in six-well plates and transfected with 1 μg/well of indicated plasmid DNA using FuGene 6 according to the manufacturer's instructions. Cells typically were left to express constructs for 24-72 hours following transfection (as assessed by microscopy) and were used between 24 and 48 hours post transfection for all FLIM studies. Before imaging, cells were plated on glass coverslips or Mattek dishes (for line experiments) coated with extracellular matrix proteins or poly-L-lysine (Sigma) as indicated.

Bead coating and incubation

4 μm latex beads (Dynal) were washed in PBS and incubated with diluted proteins or antibodies as stated in figure legends at indicated concentrations. Anti-β1 monoclonal antibodies used in the study are: K20 (neutral); (Amiot et al., 1986; Mould et al., 2005), 12G10 (activating) (Mould et al., 1995; Mould et al., 2002) or mAb13 (inactivating) (Akiyama et al., 1989) and were all generated in-house as previously described. Beads were left overnight at 4°C to allow even protein binding, and subsequently washed three times and re-suspended in PBS to form a 50% slurry final concentration. Plated cells were incubated with 5 μl/ml of beads in growth media and incubated at 37°C for 30 minutes. Cells were then washed three times in medium and either fixed for FLIM analysis or imaged live in phenol-red free growth media at 37°C. For integrin antagonist studies, cells were pre-treated with concentrations and times specified in figure legend with V0519 (Peyman et al., 2000), S9916197 (Gläsner et al., 2005) or S976162 (Lin et al., 1999) and subjected to FLIM analysis.

Fluorescence lifetime measurements by time-correlated single photon counting (TCSPC) FLIM

Here we used FLIM to measure FRET between protein pairs, which allows the determination of spatial protein interactions (Parsons et al., 2005). Time-domain FLIM was performed with a multi-photon microscope system as described previously (Parsons et al., 2005; Peter et al., 2005). The system is based on a modified Bio-Rad MRC 1024MP workstation, comprising a solid-state-pumped femtosecond Ti:Sapphire (Tsunami, Spectra-Physics) laser system, a focal scan-head and an inverted microscope (Nikon TE200). Enhanced detection of the scattered component of the emitted (fluorescence) photons was afforded by the use of fast response (Hamamatsu R7401-P) non-descanned detectors, developed in-house, situated in the re-imaged objective pupil plane. Fluorescence lifetime imaging capability was provided by time-correlated single photon counting electronics (Becker & Hickl, SPC 700). A 40× objective was used throughout (Nikon, CFI60 Plan Fluor NA 1.3) and data collected at 500±20 nm through a bandpass filter (Coherent Inc., 35-5040). Laser power was adjusted to give average photon counting rates of the order 10^4-10^5 photons (0.0001 to 0.001 photon counts per excitation event) to avoid pulse pile up. Acquisition times up to 300 seconds at low excitation power were used to achieve sufficient photon statistics for fitting, while avoiding either pulse pile-up or significant photobleaching. Excitation was at 890 nm. Widefield acceptor (mRFP) images were acquired using a CCD camera (Hammamatsu) at <100 millisecond exposure times.

Analysis of data for FRET experiments

Data were analysed as previously described (Parsons et al., 2005; Prag et al., 2007). Briefly, bulk measurements of FRET efficiency (i.e. intensity-based methods) cannot distinguish between an increase in FRET efficiency (i.e. coupling efficiency) and an increase in FRET population (concentration of FRET species) since the two parameters are not resolved. Measurements of FRET based on analysis of the fluorescence lifetime of the donor can resolve this issue when analyzed using multi-exponential decay models. For measurements of bulk interactions (i.e. where only single exponential decays are fit to the data), measured efficiencies will appear significantly lower because of the assumption that all donors are associated with one or more acceptors. The assumption that non-interacting and interacting fractions are present allows the determination of the efficiency of interaction. The FRET efficiency is related to the molecular separation of donor and acceptor and the fluorescence lifetime of the interacting fraction by:

$$n_{fret} = [R_0^6 / (R_0^6 + r^6)] = 1 - n_{fret} / \tau_d ,$$

where R_0 is the Förster radius, r the molecular separation, n_{fret} is the lifetime of the interacting fraction and τ_d the lifetime of the donor in the absence of acceptor. n_{fret} and τ_d can also be taken to be the lifetime of the interacting fraction and non-interacting fraction, respectively. All data were analysed using TRI2 software [developed by Paul Barber, Gray Cancer Institute, London, UK (Prag et al., 2007); supplementary material Fig. S3]. For the analysis of FRET at the bead interface, a mask of constant defined pixel size was placed over individual bead areas and the lifetimes analysed and calculated within that area alone (see supplementary material Fig. S3). Histogram data presented here are plotted as mean FRET efficiency from >10 cells per sample. Average FRET efficiency is shown ± s.e.m. ANOVA was used to test statistical significance between different populations of data. Lifetime images of example cells are presented using a pseudocolour scale whereby blue depicts normal GFP lifetime (no FRET) and red depicts lower GFP lifetime (areas of FRET).

Confocal microscopy

Cells were permeabilised with 0.2% (v/v) Triton-X-100/PBS following fixation in 4% (w/v) paraformaldehyde. Primary antibodies or phalloidin were diluted 1:200-1:500 in phosphate-buffered saline containing 1% (w/v) BSA. The FITC- and Cy3-labelled secondary conjugates were obtained from Jackson ImmunoResearch Laboratories. Confocal images were acquired on a confocal laser-scanning microscope (model LSM 510 Meta, Carl Zeiss Inc.) equipped with both 40×/1.3 Plan-Neofluar and 63×/1.4 Plan-APOCHROMAT oil-immersion objectives.

The authors would like to thank Simon Ameer-Beg, Boris Vojnovic and Paul Barber for their continued support and development of the multiphoton FLIM system and software. The authors are also grateful to Sanofi-Aventis (Frankfurt) for providing the inhibitor compounds. This work was supported by a Royal Society University Research Fellowship (to M.P.) and grants 045225 and 074941 from the Wellcome Trust (to M.J.H.).

References

Akiyama, S. K., Yamada, S. S., Chen, W. T. and Yamada, K. M. (1989). Analysis of fibronectin receptor function with monoclonal antibodies: roles in cell adhesion, migration, matrix assembly, and cytoskeletal organization. *J. Cell Biol.* **109**, 863-875.

Amiot, M., Bernard, A., Tran, H. C., Leca, G., Kanellopoulos, J. M. and Boumsell, L. (1986). The human cell surface glycoprotein complex (gp 120,200) recognized by monoclonal antibody K20 is a component binding to phytohaemagglutinin on T cells. *Scand. J. Immunol.* **23**, 109-118.

Ballestrem, C., Hinz, B., Imhof, B. A. and Wehrle-Haller, B. (2001). Marching at the front and dragging behind : differential Vβ3-integrin turnover regulates focal adhesion behavior. *J. Cell Biol.* **155**, 1319-1332.

Calderwood, D. A., Zent, R., Grant, R., Rees, D. J., Hynes, R. O. and Ginsberg, M. H. (1999). The talin head domain binds to integrin subunit cytoplasmic tails and regulates integrin activation. *J. Biol. Chem.* **274**, 28071-28074.

Garcia-Alvarez, B., de Pereda, J. M., Calderwood, D. A., Ulmer, T. S., Critchley, D., Campbell, I. D., Ginsberg, M. H. and Liddington, R. C. (2003). Structural determinants of integrin recognition by Talin. *Mol. Cell* **11**, 49-58.

Gläsner, J., Blum, H., Wehner, V., Stilz, H. U., Humphries, J. D., Curley, G. P., Mould, A. P., Humphries, M. J., Hallmann, R., Röllinghoff, M. et al. (2005). A small molecule alpha 4 beta 1 antagonist prevents development of murine Lyme arthritis without affecting protective immunity. *J. Immunol.* **175**, 4724-4734.

Goldfinger, L. E., Han, J., Kiosses, W. B., Howe, A. K. and Ginsberg, M. H. (2003). Spatial restriction of 4 integrin phosphorylation regulates lamellipodial stability and 4β1-dependent cell migration. *J. Cell Biol.* **162**, 731-741.

Graus-Porta, D., Blaess, S., Senften, M., Littlewood-Evans, A., Damsky, C., Huang, Z., Orban, P., Klein, R., Schittny, J. C. and Muller, U. (2001). Beta1-class integrins regulate the development of laminae and folia in the cerebral and cerebellar cortex. *Neuron* **31**, 367-379.

Hantgan, R. R., Stahle, M. C., Connor, J. H., Connor, R. F. and Mousa, S. A. (2007). αIIbβ3 priming and clustering by orally active and intravenous integrin antagonists. *J. Thromb. Haemost.* **5**, 542-550.

Humphries, M. J. (2000). Integrin structure. *Biochem. Soc. Trans.* **28**, 311-339.

Hynes, R. O. (2002). Integrins: bi-directional, allosteric, signaling machines. *Cell* **110**, 673-687.

Jat, P. S., Noble, M. D., Ataliotis, P., Tanaka, Y., Yannoutsos, N., Larsen, L. and Kioussis, D. (1991). Direct derivation of conditionally immortal cell lines from an H-2Kb-tsA58 transgenic mouse. *Proc. Natl. Acad. Sci. USA* **88**, 5096-5100.

Kim, M., Carman, C. V. and Springer, T. A. (2003). Bidirectional transmembrane signaling by cytoplasmic domain separation in integrins. *Science* **301**, 1720-1725.

Leclerc, J. R. (2002). Platelet glycoprotein IIb/IIIa antagonists: lessons learned from clinical trials and future directions. *Crit. Care Med.* **30**, S332-S340.

Lin, K., Ateeq, H. S., Hsiung, S. H., Chong, L. T., Zimmerman, C. N., Castro, A., Lee, W. C., Hammond, C. E., Kalkunte, S., Chen, L. L. et al. (1999). Selective, tight-binding inhibitors of integrin alpha4beta1 that inhibit allergic airway responses. *J. Med. Chem.* **42**, 920-934.

Liu, S., Thomas, S. M., Woodside, D. G., Rose, D. M., Kiosses, W. B., Pfaff, M. and Ginsberg, M. H. (1999). Binding of paxillin to alpha4 integrins modifies integrin-dependent biological responses. *Nature* **402**, 676-681.

Luo, B. H., Carman, C. V. and Springer, T. A. (2007). Structural basis of integrin regulation and signaling. *Annu. Rev. Immunol.* **25**, 619-647.

Mould, A. P., Garratt, A. N., Askari, J. A., Akiyama, S. K. and Humphries, M. J. (1995). Identification of a novel anti-integrin monoclonal antibody that recognises a ligand-induced binding site epitope on the beta 1 subunit. *FEBS Lett.* **363**, 118-122.

Mould, A. P., Askari, J. A., Barton, S., Kline, A. D., McEwan, P. A., Craig, S. E. and Humphries, M. J. (2002). Integrin activation involves a conformational change in the 1 helix of the subunit a-domain. *J. Biol. Chem.* **277**, 19800-19805.

Mould, A. P., Travis, M. A., Barton, S. J., Hamilton, J. A., Askari, J. A., Craig, S. E., McDonald, P., Kammerer, R. A., Buckley, P. A. and Humphries, M. J. (2005). Evidence that monoclonal antibodies directed against the integrin subunit plexin/semaphorin/integrin domain stimulate function by inducing receptor extension. *J. Biol. Chem.* **280**, 4238-4246.

Mousa, S. A. (2002). Anti-integrin as novel drug-discovery targets: potential. therapeutic and diagnostic implications. *Curr. Opin. Chem. Biol.* **6**, 534-541.

Newham, P., Craig, S. E., Clark, K., Mould, A. P. and Humphries, M. J. (1998). Analysis of ligand-induced and ligand-attenuated epitopes on the leukocyte integrin alpha4beta1: VCAM-1, mucosal addressin cell adhesion molecule-1, and fibronectin induce distinct conformational changes. *J. Immunol.* **160**, 4508-4517.

Otey, C. A., Pavalko, F. M. and Burridge, K. (1990). An interaction between a-actinin and the b-1 integrin subunit in vitro. *J. Cell Biol.* **111**, 721-729.

Parsons, M., Monypenny, J., Ameer-Beg, S. M., Millard, T. M., Machesky, L. M., Peter, M., Chernoff, J., Zicha, D., Vojnovic, B. and Ng, T. (2005). Spatially distinct binding of Cdc42 to PAK1 and N-WASP in breast carcinoma cells. *Mol. Cell. Biol.* **25**, 1680-1695.

Peter, M., Ameer-Beg, S. M., Hughes, M. K., Keppler, M. D., Prag, S., Marsh, M., Vojnovic, B. and Ng, T. (2005). Multiphoton-FLIM quantification of the EGFP-mRFP1 FRET pair for localization of membrane receptor-kinase interactions. *Biophys. J.* **88**, 1224-1237.

Peyman, A., Wehner, V., Knolle, J., Stilz, H. U., Breipohl, G., Scheunemann, K. H., Carniato, D., Ruxer, J. M., Gourvest, J. F., Gadek, T. R. et al. (2000). RGD mimetics containing a central hydantoin scaffold: (v)β3 *vs* (IIb)β3 selectivity requirements. *Bioorg. Med. Chem. Lett.* **10**, 179-182.

Prag, S., Parsons, M., Keppler, M. D., Ameer-Beg, S. M., Barber, P., Hunt, J., Beavil, A. J., Calvert, R., Arpin, M., Vojnovic, B. et al. (2007). Activated ezrin promotes cell migration through recruitment of the gef dbl to lipid rafts and preferential downstream activation of Cdc42. *Mol. Biol. Cell* **18**, 2935-2948.

Schaller, M. D., Otey, C. A., Hildebrand, J. D. and Parsons, J. T. (1995). Focal adhesion kinase and paxillin bind to peptides mimicking beta integrin cytoplasmic domains. *J. Cell Biol.* **130**, 1181-1187.

Tadokoro, S., Shattil, S. J., Eto, K., Tai, V., Liddington, R. C., de Pereda, J. M., Ginsberg, M. H. and Calderwood, D. A. (2003). Talin binding to integrin tails: a final common step in integrin activation. *Science* **302**, 103-106.

Tremuth, L., Kreis, S., Melchior, C., Hoebeke, J., Ronde, P., Plancon, S., Takeda, K. and Kieffer, N. (2004). A fluorescence cell biology approach to map the second integrin-binding site of talin to a 130-amino acid sequence within the rod domain. *J. Biol. Chem.* **279**, 22258-22266.

van der Neut, R., Krimpenfort, P., Calafat, J., Niessen, C. M. and Sonnenberg, A. (1996). Epithelial detachment due to absence of hemidesmosomes in integrin beta4 null mice. *Nat. Genet.* **13**, 366-369.

Wagner, N., Lohler, J., Kunkel, E. J., Ley, K., Leung, E., Krissansen, G., Rajewsky, K. and Muller, W. (1996). Critical role for 137 integrins in formation of the gut-associated lymphoid tissue. *Nature* **382**, 366-370.

Xing, B., Jedsadayanmata, A. and Lam, S. C. (2001). Localization of an integrin binding site to the C terminus of talin. *J. Biol. Chem.* **276**, 44373-44378.

Zhang, H., Berg, J. S., Li, Z., Wang, Y., Lang, P., Sousa, A. D., Bhaskar, A., Cheney, R. E. and Stromblad, S. (2004). Myosin-X provides a motor-based link between integrins and the cytoskeleton. *Nat. Cell Biol.* **6**, 523-531.